Fringe-Field Switching with a Negative Dielectric Anisotropy Liquid Crystal

Yuan Chen, Zhenyue Luo, Fenglin Peng, and Shin-Tson Wu, *Fellow, IEEE*

Abstract—We report a high performance negative dielectric anisotropy ($\Delta\varepsilon$) liquid crystal for fringing field switching (n-FFS) display. We compare the electro-optic characteristics of FFS cells using positive and negative $\Delta\varepsilon$ LCs. With comparable driving voltage and response time, the n-FFS cell has advantages in higher transmittance, single gamma curve, less cell gap sensitivity and slightly wider viewing angle. LC director deformation distribution is analyzed to explain these performance differences.

Index Terms—Fringe field switching, liquid crystal displays (LCD).

TABLE I
PHYSICAL PROPERTIES OF THREE LCs STUDIED (T = 23 °C, λ = 633 nm AND f = 1 kHz)

LC	T_c(°C)	Δn	γ_1 (mPa.s)	$\Delta\varepsilon$
MLC-6882	69	0.097	108	-3.1
UCF-N1	73.3	0.116	122.8	-3.82
MLC-6686	71	0.097	102	10
UCF-P1	73.3	0.116	122.8	10

I. INTRODUCTION

MOBILE displays, such as smartphones and tablet computers, have become indispensable in our daily life. Wide viewing angle for many simultaneous observers, high resolution for Retina display, low power consumption for long battery life, and pressure-resistance for touch screen are the key requirements. Fringe field switching (FFS) [1]–[5] liquid crystal display (LCD), in which the electric-field-induced molecular reorientation takes place mainly in the horizontal direction, satisfies the above criteria and is commonly used in these display devices.

Presently, most FFS LCDs use positive dielectric anisotropy ($\Delta\varepsilon$) liquid crystals (LCs). The primary reason is that it is relatively easy to obtain a large $\Delta\varepsilon(\sim 10)$ while keeping a low viscosity. Large $\Delta\varepsilon$ helps to reduce operation voltage while low viscosity helps to shorten response time. However, positive LC-based FFS (p-FFS) displays exhibit some problems: 1) its peak transmittance is limited to ~88%; 2) the voltage-dependent transmittance (VT) curves do not overlap well for RGB colors. Thus, three gamma curves are required, which increases the complexity of driving electronics; 3) the electro-optic effects are sensitive to the cell gap, and 4) a small but noticeable image flickering due to splay-induced flexoelectric effect [6].

To overcome these problems, in this letter we report a FFS mode using a high performance negative $\Delta\varepsilon$ LC (n-FFS). The n-FFS mode has been investigated previously [1], [7], [8], but mainly by simulations. In this paper, we report a negative $\Delta\varepsilon$ LC mixture with relatively high birefringence and low viscosity. In comparison to p-FFS, our n-FFS exhibits several outstanding features, such as higher transmittance, single gamma curve for red, green and blue pixels, cell gap insensitivity, slightly faster

response time, and comparable on-state voltage although the negative LC usually has a smaller dielectric anisotropy. Therefore, n-FFS could be a strong contender for next-generation mobile display devices.

II. EXPERIMENT

In experiment, we prepared a negative $\Delta\varepsilon$ LC mixture, named UCF-N1. It consists of 60 wt.% MLC-6882 (a low viscosity Merck mixture), 18% lateral difluoro akoxy-biphenyl, 17% lateral difluoro cyclohexane-biphenyl [9] and 5% bicyclehexane compounds. We compare our results with MLC-6882 and a positive $\Delta\varepsilon$ LC (UCF-P1) with $\Delta\varepsilon = 10$ while other properties remain the same as UCF-N1. For reference, we also include a low viscosity positive $\Delta\varepsilon$ LC mixture MLC-6686 (Merck), whose $\Delta\varepsilon = 10$, $\Delta n = 0.097$, $\gamma_1 = 102$ mPas. Table I summarizes the physical properties of these four mixtures.

To investigate the electro-optical performances at different wavelength, we measured the birefringence dispersion for MLC-6882 and UCF-N1, as shown in Fig. 1. The dots are the measured data and solid lines are the fitting results using single-band birefringence dispersion model [10]:

$$\Delta n = \frac{G\lambda^2\lambda^{*2}}{(\lambda^2 - \lambda^{*2})}, \tag{1}$$

where λ^* is the average resonant wavelength of the LC and G is a proportionality constant. Through fitting, we obtained $G = 2.82$ μm^{-2}, $\lambda^* = 177.5$ nm and $G = 2.10$ μm^{-2}, $\lambda^* = 218.4$ nm for MLC-6682 and UCF-N1, respectively. With a higher Δn, UCF-N1 has a longer resonant wavelength as expected. With these fitting parameters, the birefringence at a desired wavelength can be calculated through (1).

III. SIMULATION

The electro-optical properties of both n-FFS and p-FFS are calculated by a commercial LCD simulator DIMOS.2D and the extended Jones matrix [11]. As will be shown later, the preferred $d\Delta n$ value for achieving high transmittance at $\lambda = 550$ nm and fast response time is ~360 nm for n-FFS and ~380 nm for
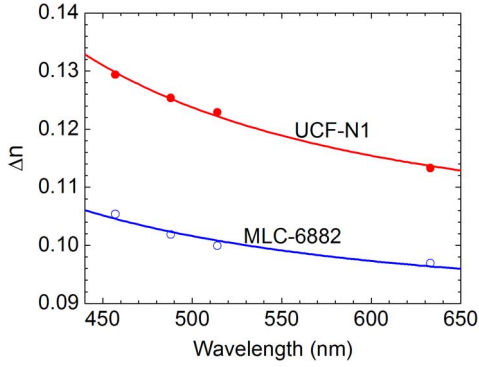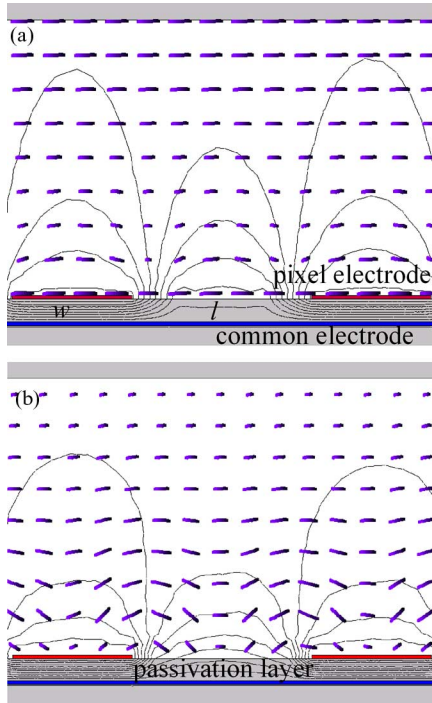
75

Fig. 1.   Birefringence dispersion of MLC-6882 and UCF-N1.

Fig. 2.   Device configuration of FFS structure, equal-potential lines, and LC director deformation of (a) n-FFS and (b) p-FFS.

Fig. 3.   VT curves for (a) FFS-N1 and (b) FFS-P1. The inset plots show the normalized VT curves.

p-FFS. This difference results from the more efficient LC director reorientation in the n-FFS. To make a fair comparison between n-FFS and p-FFS, we use the same electrode width $w = 2\ \mu$m and gap $l = 3\ \mu$m, same pretilt angle (2°) but the rubbing angle is 10° and 80°, respectively, w.r.t. the horizontal axis. Fig. 2(a) and 2(b) shows the device configuration, calculated equal-potential lines and LC director deformation in a voltage-on state. The passivation layer between the pixel and common electrodes is SiO_x whose thickness is $d_p = 250$ nm and dielectric constant is $\varepsilon_p = 4.5$ [7]. The cell is sandwiched between two crossed linear polarizers, and the transmission axis of the bottom polarizer is parallel to the rubbing direction.

1) VT Curves: Fig. 3(a) depicts the simulated VT curves for n-FFS using UCF-N1 ($\Delta n = 0.119$ at $\lambda = 550$ nm) with cell gap $d = 3.02\ \mu$m. For convenience, let us call it FFS-N1. The peak transmittance (T_p) of FFS-N1 reaches ~98% ($\lambda = 550$ nm) at the on-state voltage $V_{on} = 4.6$ V. Moreover, both
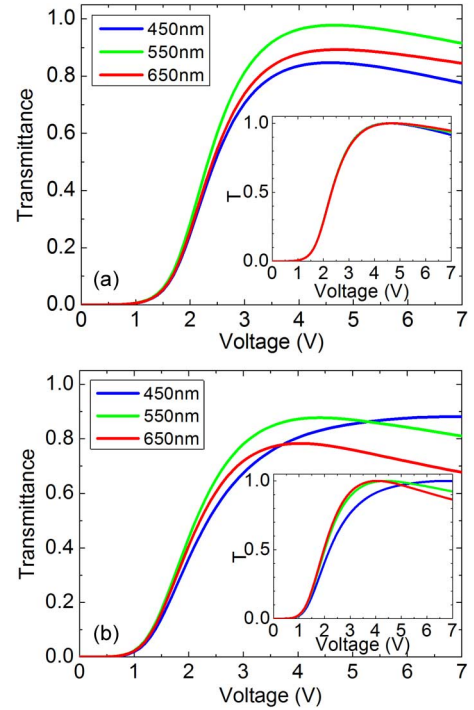
RGB colors have nearly the same V_{on}. The inset plot shows the normalized VT curves and they overlap amazingly well. Thus, a single gamma curve driving can be realized for n-FFS, which would simplify the driving circuit.

For comparison, we also calculate the VT curves of a p-FFS cell $(d = 3.19\ \mu$m) using UCF-P1. Let us call it FFS-P1. Results are shown in Fig. 3(b). The dispersion of VT curves for RGB colors is quite noticeable. At 550 nm, T_p reaches ~88% and $V_{on} = 4.4$ V. The V_{on} for 650 nm is 4.0 V and $T_p = 78.3\%$. For $\lambda = 450$ nm, T_p can reach 88.1%, but at a much higher voltage (6.8 V). The inset plot in Fig. 3(b) depicts the normalized VT curves. Obviously, they do not overlap well. Thus, three different gamma curves are needed to drive the RGB pixels.

2) LC Director Deformation Distribution: In order to better understand the transmittance and gamma curve differences, we investigate the LC twist and tilt angle distribution for both FFS-N1 and FFS-P1 at five positions (A to E as Fig. 4(a) shows). To obtain maximum phase retardation, the twist angle should occur at 45°. From Fig. 4, the LC directors are largely twisted near the bottom of the cell ($z/d < 0.4$) by the electric field and gradually reoriented back to the rubbing direction due to the anchoring force provided by the top surface. For FFS-N1, the maximum twist angle from the initial rubbing direction is around 46° at A and E. The tilt angle at A and E is close to 0, which contributes effectively to the phase retardation. At B, C, and D, the horizontal electric field is stronger and the maximum twist angle is $\sim 55°$. Meanwhile, the tilt angle at $z/d \sim 0.1$ is $\sim \pm 10°$, which would slightly decrease the phase retardation and compensate the over twist. Moreover, the on-state n-FFS cell is like two cascaded TN cells [12] due to the small tilt

Fig. 5. $d\Delta n$ effects on V_{on} and T_p of FFS-N1 and FFS-P1. $\lambda = 550$ nm.
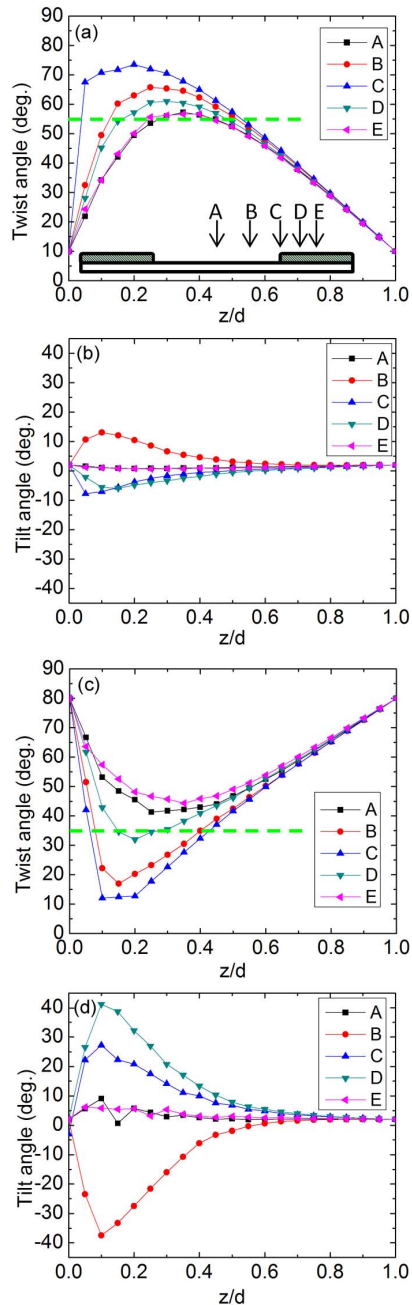

Fig. 4. Simulated twist angle distribution of (a) FFS-N1 and (c) FFS-P1; Tilt angle distribution of (b) FFS-N1 and (d) FFS-P1.

angle. As a result, polarization rotation effects dominates and the color dispersion is suppressed.

In contrast, the maximum twist angle of FFS-P1 is either larger than 63° (B and C) or smaller than 38° (A and E). The over- or under-twist leads to inefficient phase retardation. Only at position D, the maximum twist angle is about 48°, however the tilt angle is about 41° at z/d = 0.1. The large tilt angle caused by the strong vertical field dramatically decreases the effective birefringence and hence the peak transmittance. Meanwhile, with a large tilt angle at positions B, C, and D, the phase retardation effect (which is wavelength sensitive) becomes quite obvious, resulting in a severe wavelength dispersion. Also from
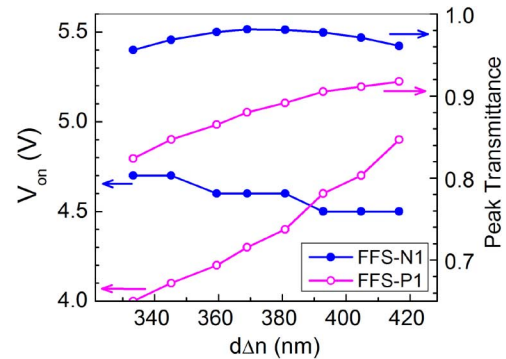
Fig. 2(b), splay deformation occurs and electric polarization is induced, which is known as flexoelectric effect [6]. The light transmittance would differ from negative to positive frames, resulting in a small image flickering. By contrast, this effect is negligible in n-FFS due to the small tilt angle.

As Fig. 3 shows, FFS-P1 has a lower threshold voltage than FFS-N1 because its $\Delta\varepsilon$ (+10) is much larger than that of UCF-N1 (−3.82), assuming their K_{22} is the same. However, the on-state voltage of FFS-P1 ($V_{on} \sim 4.4$ V) is nearly the same as that of FFS-N1 (4.6 V). This can be explained by the LC director distributions shown in Figs. 4(a)–(d). FFS-N1 has more efficient twist angle ($\sim 45°$) and smaller tilt angle than FFS-P1 so that its effective birefringence is higher. As a result, a smaller voltage swing ($\Delta V = V_{on} - V_{th}$) is needed to reach the peak transmittance. Therefore, FFS-N1 has a comparable V_{on} to FFS-P1, although its $\Delta\varepsilon$ is much smaller.

3) Response Time: Both rise time and decay time are calculated between the 10% and 90% transmittance change. For FFS-P1 with d = 3.19 μm, the simulated [rise time, decay time] is [23.8 ms, 25.7 ms]. With MLC-6686 (d = 3.87 μm), the calculated [rise time, decay time] at V_{on} = 5.4 V is [26.8 ms, 29.7 ms]. For the n-FFS cell with MLC-6882 ($d = 3.66$ μm and V_{on} = 4.5 V) the simulated [rise time, decay time] is [23.4 ms, 34.8 ms]. With our UCF-N1 ($d = 3.02$ μm), the calculated [rise time, decay time] is [16.2 ms, 24.1 ms]. Our UCF-N1 has faster response time than MLC-6882 because of its thinner cell gap. On the other hand, UCF-N1 has faster response time than FFS-P1 due to its more uniform twist and tilt angles. A lower viscosity LC would further reduce the response time. For example, if the viscosity of UCF-P1 is decreased to 80 mPas, then the simulated [rise time, decay time] would decrease to [15.6 ms, 16.8 ms].

4) Cell Gap Effect: For high yield manufacturing, it is desirable to keep the cell gap above 3 μm. Fig. 5 shows the $d\Delta n$ effects on T_p and V_{on} for both FFS-N1 and FFS-P1 at $\lambda = 550$ nm. For FFS-N1, both T_p and V_{on} are quite inert to the $d\Delta n$ variation in the 360–390 nm range. Since the Δn of our LC is 0.119, we chose $d\Delta n \sim 360$ nm, i.e., d = 3.02 μm for achieving fast response time. By contrast, in the same range the V_{on} of FFS-P1 climbs almost linearly from 4.2 V to 4.6 V and T_p increases from 86% to 91%. For FFS-P1, we chose $d\Delta n \sim 380$ nm to compromise the performance between transmittance, V_{on} and response time.
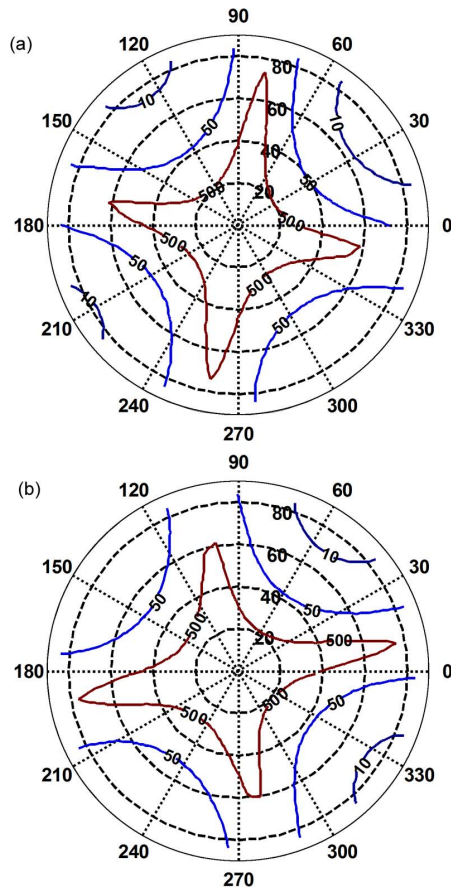
Fig. 6.   Simulated isocontrast plots for: (a) FFS-P1 and (b) FFS-N1.

5) Viewing Angle: We also compare the viewing angle for the FFS cells using both positive and negative $\Delta\varepsilon$ LCs. Figs. 6(a) and 6(b) show the isocontrast plot for FFS-P1 and FFS-N1. Since their dark states are similar due to the same alignment, the contrast ratio (CR) is mainly determined by the bright state. FFS-N1 has a slightly better isocontrast performance due to its higher transmittance and more uniform in-plane director twist and small tilt angle in the bright state. To achieve wide view, various compensation films for FFS mode have been developed [13], [14]. With one biaxial film, a CR over 100:1 can be achieved in almost the entire viewing zone ($\pm 80°$). To further widen the viewing angle, multi-domain structures can be considered [3].

IV. DISCUSSION

Besides high transmittance, low driving voltage also helps to reduce power consumption and prolong the battery life. In FFS mode, the capacitor formed by the passivation layer between the pixel and common electrode acts as a storage capacitor ($Cs \sim \varepsilon_p A_{pixel}/d_p$), which is in parallel to the LC capacitor. One possible approach to lower V_{on} is to use a thin and large ε_p dielectric layer for increasing Cs and reducing the voltage shielding effect [15]. For example, if we reduce the SiO_x layer thickness from 250 nm to 100 nm, then V_{on} would decrease from 4.6 V to 3.9 V. A tradeoff is the increased charging

time resulting from the increased Cs. But for a high resolution mobile display, its pixel size is small so that Cs can still be kept relatively small for quick addressing. Another approach is to reduce the rubbing angle [16]. Together with 5° rubbing angle and 100-nm SiO_x passivation layer, V_{on} can be reduced to 3.5 V.

V. CONCLUSION

We have demonstrated a new negative $\Delta\varepsilon$ LC mixture with modest birefringence and low viscosity for FFS LCDs. Our n-FFS shows superior performances to p-FFS in following aspects: 1) higher transmittance (98% versus 88%); 2) single gamma curve for RGB pixels; 3) both on-state voltage and peak transmittance are less sensitive to cell gap variation, 4) slightly wider viewing angle; 5) faster response time due to a slightly thinner cell gap and more uniform LC twist and tilt angles, and 6) comparable on-state voltage to p-FFS although the LC mixture has a smaller $\Delta\varepsilon$ (-3.8 versus $+10$). Therefore, n-FFS has potential to replace p-FFS for next-generation mobile displays.

REFERENCES

[1] S. H. Lee, S. L. Lee, S. H. Lee, and H. Y. Kim, "Electro-optic characteristics and switching principle of a nematic liquid crystal cell controlled by fringe-field switching," *Appl. Phys. Lett.*, vol. 73, pp. 2881–2883, 1998.

[2] S. H. Lee, S. L. Lee, H. Y. Kim, and T. Y. Eom, "A novel wide-viewing-angle technology: Ultra-Trans View," in *SID Symp. Dig.*, 1999, vol. 30, pp. 202–205.

[3] S. H. Lee, S. M. Lee, H. Y. Kim, J. M. Kim, S. H. Hong, Y. H. Jeong, C. H. Park, Y. J. Choi, J. Y. Lee, J. W. Koh, and H. S. Park, "Ultra-FFS TFT-LCD with super image quality and fast response time," in *SID Symp. Dig.*, 2001, vol. 32, pp. 484–487.

[4] S. H. Lee, H. Y. Kim, S. M. Lee, S. H. Hong, J. M. Kim, J. W. Koh, J. Y. Lee, and H. S. Park, "Ultra-FFS TFT-LCD with super image quality, fast response time, strong pressure-resistant characteristics," *J. Soc. Inf. Disp.*, vol. 10, pp. 117–122, 2002.

[5] H. Y. Kim, S. H. Nam, and S. H. Lee, "Dynamic stability of the fringe-field switching liquid crystal cell depending on dielectric anisotropy of a liquid crystal," *Jpn. J. Appl. Phys.*, vol. 42, pp. 2752–2755, 2003.

[6] L. M. Blinov and V. G. Chigrinov, *Electrooptic Effects in Liquid Crystal Materials*.   : Springer-Verlag, 1994.

[7] Z. Ge, X. Zhu, T. X. Wu, and S. T. Wu, "High transmittance in-plane-switching liquid crystal displays," *J. Display Technol.*, vol. 2, pp. 114–120, 2006.

[8] H. J. Yun, M. H. Jo, I. W. Jang, S. H. Lee, S. H. Ahn, and H. J. Hur, "Achieving high light efficiency and fast response time in fringe field switching mode using a liquid crystal with negative dielectric anisotropy," *Liq. Cryst.*, vol. 39, pp. 1141–1148, 2012.

[9] M. Hird, "Florinated liquid crystals-properties and applications," *Chem. Soc. Rev.*, vol. 36, pp. 2070–2095, 2007.

[10] S. T. Wu, "Birefringence dispersions of liquid crystals," *Phys. Rev. A*, vol. 33, pp. 1270–1274, 1986.

[11] A. Lien, "Extended Jones matrix representation for the twisted nematic liquid-crystal display at oblique-incidence," *Appl. Phys. Lett.*, vol. 57, pp. 2767–2769, 1990.

[12] Z. Ge, S. T. Wu, S. S. Kim, J. W. Park, and S. H. Lee, "Thin cell fringe-field-switching liquid crystal display with a chiral dopant," *Appl. Phys. Lett.*, vol. 92, p. 181109, 2008.

[13] R. Lu, X. Zhu, S. T. Wu, Q. Hong, and T. X. Wu, "Ultrawide-view liquid crystal displays," *J. Display Technol.*, vol. 1, no. 1, pp. 3–14, Sep. 2005.

[14] X. Zhu, Z. Ge, and S. T. Wu, "Analytical solutions for uniaxial-film-compensated wide-view liquid crystal displays," *J. Display Technol.*, vol. 2, no. , pp. 2–20, 2006.

[15] M. Jiao, Z. Ge, Q. Song, and S. T. Wu, "Alignment layer effects on thin liquid crystal cells," *Appl. Phys. Lett.*, vol. 92, p. 061102, 2008.

[16] S. H. Hong, I. C. Park, H. Y. Kim, and S. H. Lee, "Electro-optic characteristic of fringe-field switching mode depending on rubbing direction," *Jpn. J. Appl. Phys.*, vol. 39, pp. L527–L530, 2000.